

High-resolution climate simulation of the last glacial maximum

Seong-Joong Kim · Thomas J. Crowley ·
David J. Erickson · Bala Govindasamy ·
Phillip B. Duffy · Bang Yong Lee

Received: 13 December 2006 / Accepted: 17 October 2007 / Published online: 6 November 2007
© Springer-Verlag 2008

Abstract The climate of the last glacial maximum (LGM) is simulated with a high-resolution atmospheric general circulation model, the NCAR CCM3 at spectral truncation of T170, corresponding to a grid cell size of roughly 75 km. The purpose of the study is to assess whether there are significant benefits from the higher resolution simulation compared to the lower resolution simulation associated with the role of topography. The LGM simulations were forced with modified CLIMAP sea ice distribution and sea surface temperatures (SST) reduced by 1°C, ice sheet topography, reduced CO₂, and

21,000 BP orbital parameters. The high-resolution model captures modern climate reasonably well, in particular the distribution of heavy precipitation in the tropical Pacific. For the ice age case, surface temperature simulated by the high-resolution model agrees better with those of proxy estimates than does the low-resolution model. Despite the fact that tropical SSTs were only 2.1°C less than the control run, there are many lowland tropical land areas 4–6°C colder than present. Comparison of T170 model results with the best constrained proxy temperature estimates (noble gas concentrations in groundwater) now yield no significant differences between model and observations. There are also significant upland temperature changes in the best resolved tropical mountain belt (the Andes). We provisionally attribute this result in part as resulting from decreased lateral mixing between ocean and land in a model with more model grid cells. A longstanding model-data discrepancy therefore appears to be resolved without invoking any unusual model physics. The response of the Asian summer monsoon can also be more clearly linked to local geography in the high-resolution model than in the low-resolution model; this distinction should enable more confident validation of climate proxy data with the high-resolution model. Elsewhere, an inferred salinity increase in the subtropical North Atlantic may have significant implications for ocean circulation changes during the LGM. A large part of the Amazon and Congo Basins are simulated to be substantially drier in the ice age—consistent with many (but not all) paleo data. These results suggest that there are considerable benefits derived from high-resolution model regarding regional climate responses, and that observationalists can now compare their results with models that resolve geography at a resolution comparable to that which the proxy data represent.

S.-J. Kim (✉) · B. Y. Lee
Korea Polar Research Institute, KORDI,
PO Box 32, Incheon 406-840, South Korea
e-mail: seongjkim@kopri.re.kr

B. Y. Lee
e-mail: bylee@kopri.re.kr

T. J. Crowley
School of Geosciences, Grant Institute,
The University of Edinburgh, Edinburgh EH9 3JW, UK
e-mail: thomas.crowley@ed.ac.uk

D. J. Erickson
Oak Ridge National Laboratory,
PO Box 2008, Oak Ridge, TN 37831, USA
e-mail: ericksondj@ornl.gov

B. Govindasamy · P. B. Duffy
Lawrence Livermore National Laboratory,
PO Box 808, Livermore, CA 94550, USA
e-mail: bala@llnl.gov

P. B. Duffy
e-mail: pduffy@llnl.gov

1 Introduction

The last glacial maximum (LGM) climate event peaked about 21,000 years ago and provides a great opportunity to examine mechanisms for an alternate climate that has a wealth of data for validation. Geological and geochemical proxy data have been used to provide a broad picture of the LGM climate (e.g., CLIMAP 1976, 1981). There have been many studies of the global LGM climate using several kinds of numerical models (Gates 1976; Manabe and Hahn 1977; Kutzbach and Wright 1985; Kutzbach and Guetter 1986; Hyde et al. 1989; Weaver et al. 1998; Ganopolski et al. 1998; Broccoli 2000; Joussaume and Taylor 2000; Hewitt et al. 2001; Kitoh et al. 2001; Kim et al. 2002, 2003; Shin et al. 2003; Peltier and Solheim 2004; Kageyama et al. 2006; Otto-Bliesner et al. 2006). While these modelling efforts have been useful for providing insight into many important climatological processes, the models have used relatively coarse spatial resolutions. In this study, we revisit the simulation of the LGM climate using a relatively fine resolution numerical model and investigate the climate response to the imposition of the LGM boundary conditions.

Although a fine-grid model has previously been run for the North American sector (Bromwich et al. 2004, 2005), to our knowledge this is the first application of a global model at the same high resolution. In order to investigate whether there is a difference in climate response between the high resolution and low resolution, we also performed simulations of the present and LGM climate using the low-resolution version (T42) of the CCM3 with identical boundary conditions that applied for the high-resolution version. Even though large-scale features from the high-resolution model version appear to be similar to those of low-resolution, there are clear differences in regional-scale features. This study focuses on the description of regional-scale features of the LGM climate simulated in the high-resolution model.

2 Model description and experiments

The simulations were performed with the CCM3 atmospheric general circulation model. We used a model version known as “CCM3.10.11 with 3.6.6 physics.” This has identical physics to CCM3.6.6, but the computational aspects of the model have been re-written to allow more reliable and efficient operation on massively parallel computers (Duffy et al. 2003). The CCM3.6.6 version was updated from its original version by adding a capability to calculate earth’s orbital parameters and screen height temperature, changing the algorithm to calculate solar zenith angle, modifying surface stress and solar radiation

calculations with 19 bands, and computing screen-height temperature everywhere. CCM3 is a global spectral model. It uses 18 levels in a hybrid vertical coordinate that is terrain-following at the surface and reduces to a pressure coordinate in the upper atmosphere with the model top at 2.9 hPa. Important physical processes are represented as described in detail by Kiehl et al. (1998a, b). The CCM3 includes a comprehensive model of land surface processes known as the NCAR Land Surface Model (LSM; Bonan 1998).

We performed the climate simulation with the model resolution defined by a T170 truncation, which has the transform grid of 512×256 cells with a typical grid size of about 75 km. However, the smallest resolved features are roughly 115 km, which corresponds to half a wavelength of the shortest resolved zonal wave at the equator. In the T170 model simulation, values of some parameters in the cloud and evaporation parameterizations were adjusted to minimize biases that were seen in results of simulations performed by Duffy et al. (2003) at T170 using parameter values from the T42 model; this tuning process, which is described in more detail in Duffy et al. (2003), was however less thorough than that performed on the T42 model version.

Table 1 describes the experiments analyzed in this study. The modern climate simulation, hereafter referred to as MOD, is forced by prescribed climatologically-averaged, monthly sea-surface temperatures (SSTs) and sea ice distributions provided by NCAR, a specified CO₂ concentration of 355 ppm, and contemporary land mask and topography. The second experiment, referred to as LGM, involves conditions representative of the LGM. The imposed LGM conditions are as follows.

1. The atmospheric CO₂ concentration is reduced to 200 ppm following ice core data (e.g., Petit et al. 1999; Sigenthaler et al. 2005).
2. The glacial surface topography was modified following the ICE-4G reconstruction of Peltier (1994) (Fig. 1a). The maximum height of the Laurentide ice sheet is $\sim 3,000$ m.

Table 1 Boundary conditions for the MOD and LGM experiments

Parameter	Experiment	
	MOD	LGM
SST	NCAR	CLIMAP
CO ₂	355 ppm	200 ppm
Eccentricity	0.01670°	0.01899°
Obliquity	23.441°	22.949°
Lon of Perihelion	102.72°	114.42°

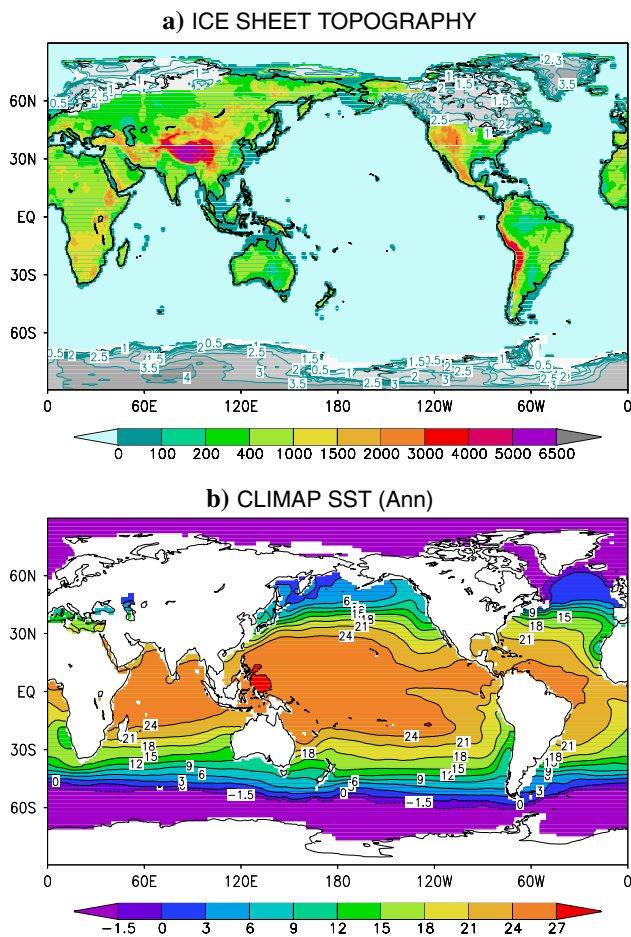


Fig. 1 Distribution of **a** the surface topography with the LGM ice sheet and **b** annual-mean sea surface temperature (SST) based on CLIMAP (1981) reconstruction. The LGM SSTs are lowered by 1°C everywhere

3. The land mask is modified to account for the lower sea level (about 120 m; cf. Fairbanks 1989; Yokoyama et al. 2000; Clark et al. 2001) as depicted by the blue color along the continental margin in Fig. 1a. Note that large areas of the western margin of the Pacific and Atlantic are exposed to land in the LGM, and that the Bering Strait is closed.
4. The lower boundary condition is a modified SST reconstruction of climatologically averaged monthly data prepared with the August and February reconstructions by CLIMAP (1981) and interpolated for the intervening intervals (Crowley and Baum 1997). Although substantial questions have been raised about the absolute value of the CLIMAP SST reconstruction (see review in Crowley 2000), the general pattern of warming and cooling has been much less disputed. More recent studies now suggest that there may be about a 1°C bias in the CLIMAP SST field (Crowley 2000; Lea 2004; Ballantyne et al. 2005). In order to

avoid the complication of ad hoc regional adjustments to the CLIMAP mask, we simply specified that LGM SSTs are lower everywhere by 1°C (Fig. 1b).

5. CLIMAP sea ice patterns were also adjusted. For the North Atlantic, a variety of data suggests that the glacial summer sea ice margin retreated into the eastern Norwegian Sea. The winter limit has also been in dispute. Our approach is to accept not new proxy SST estimates for the oceanic polar front but rather the faunal assemblage and sedimentological criteria outlined by McIntyre et al. (1976) to justify a rather extreme winter sea ice margin along 42°N that is consistent with the limit of winter ice rafted debris, the presence of polar foraminiferal assemblages, and the absence of coccolith assemblages. We base this choice on the greater reliability of sediment boundaries than that of transfer functions, confidently predicting the maximum cooling in these regions (some biota changes could be from other seasons). Even if further investigations convincingly disprove this assumption, it is useful as an end member to the range of possible sea ice distributions for the winter North Atlantic LGM. For the Southern Hemisphere, the extent of Antarctic sea ice in the Pacific sector has been reduced about 5°C of latitude, in accordance with a revised interpretation by Burckle et al. (1982; cf. Crowley and Parkinson 1988).
6. Orbital parameters are set to contemporary and 21,000 years BP according to Berger (1978) (Table 1).
7. Vegetation and soil types are unchanged except for the glaciated surfaces and land points arising due to sea-level reduction (these were assigned median vegetation and soil types for the CCM3). Although a vegetation biome overlay has been used for one ice age simulation (Crowley and Baum 1997), we believe it is best to first assess the response of the atmosphere to the physical changes in ice-age boundary condition.

3 Simulated climates

3.1 Control

The experiments were integrated for 6 years and the last 4 years were averaged and analyzed. In order to check how the model performs in simulating modern climate, the winter (December–January–February) and summer (June–July–August) precipitations and annual mean total cloud covers simulated in low-resolution (T42) and high-resolution (T170) versions are compared to observations (Fig. 2). The observed precipitation is from Xie and Arkin (1998) and cloud cover is from Warren et al. (1986, 1988). The

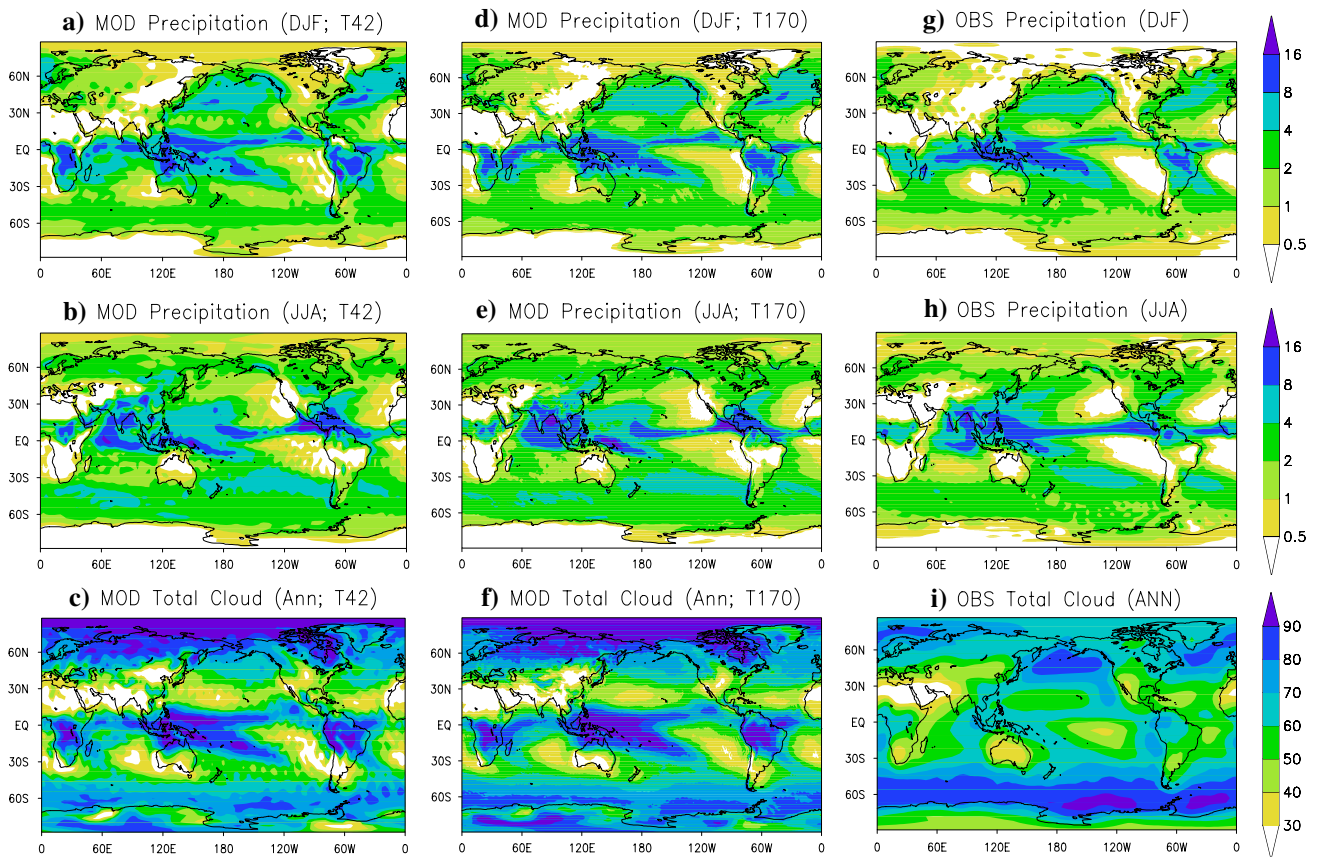


Fig. 2 Geographic distribution of the simulated **a** winter (December–January–February) and **b** summer (June–July–August) precipitation, **c** annual-mean cloud in T42, and **d** winter, **e** summer precipitation, **f** annual-mean cloud in T170, and observed **g** winter, **h** summer

precipitation, and **i** annual-mean cloud. Units are in mm day^{-1} precipitation and percent for cloud. Observed precipitation is from Xie and Arkin (1998) and cloud is from Warren et al. (1986, 1988)

spatial distribution of precipitation is a variable generally difficult to simulate in most climate models, as it depends on a number of fundamental features in the model simulation (there is almost no difference in the zonal mean precipitation between the T42 and T170). In both seasons, the model reproduces and captures the precipitation pattern found in observations reasonably well. For example, the heavy precipitation belt along the equatorial Pacific and Indian Ocean associated with strong convection in the inter-tropical convergence zone (ITCZ) is well simulated, as is the relatively low precipitation from northern Africa to the Middle East and in the eastern rims of the Pacific, Atlantic, and South Indian Ocean associated with subtropical anticyclones and strong upwelling. The maximum summer precipitation in the western Indian Ocean associated with the Asian monsoon is well captured in the simulation.

Although both model versions reproduce the present precipitation reasonably well, the high-resolution version simulates the precipitation pattern slightly better than the T42 case. For example, in DJF the heavy convective precipitation in the equatorial Pacific appears to be more realistic in the T170 than in T42 and in JJA the maximum

precipitation observed in the Bay of Bengal is well reproduced in the T170, whereas it is not that distinct in the T42 case. Even though the spatial pattern is in good agreement, the magnitude of the simulated precipitation in both versions is slightly larger than observations. This is a typical feature of the CCM3 as also shown by Hack et al. (1998) and Duffy et al. (2003). Hack et al. (1998) showed that CCM3 does a relatively poor job in simulating the tropical intraseasonal precipitation variability.

The distribution of precipitation broadly resembles the cloud cover (Fig. 2). This is particularly the case in low to mid latitudes, as would be expected. The simulated cloud cover tends to be overall overestimated in both model versions, especially in northern and southern high latitudes. An overestimation of cloud distribution in Antarctica using CCM3 is also obtained in Hines et al. (2004). In the Southern Ocean, the high-resolution version reproduces cloud cover better than the low-resolution in comparison to that of observation. Overall, CCM3 reproduces the modern precipitation and clouds in a reasonable degree and the high-resolution version of the model reproduces the features better.

3.2 LGM temperatures

Figure 3 compares the differences in annual mean surface air temperature over lands between MOD and LGM simulated in T42 version of the model with T170 version. There are both similarities and differences in surface temperature responses. For example, the surface cooling is prominent over the Laurentide and Fennoscandian ice sheets in both model versions, but the degree of surface cooling is slightly larger over the Laurentide ice sheet and smaller over Eurasia in the T42 than in the T170. Temperatures are colder in the non-glaciated region of Alaska in the T170 run. By contrast there is a tongue of relatively warm air in the south-eastern United States at T170 that does not show up at T42. The difference in surface temperature change between the two model versions in Alaska and the south-eastern United States is illustrated by the change in meridional heat flux (Fig. 4c, d). In both model versions, there is an increase in northward heat flux along the north-western rim of North America, but it is less strong in the T170 case. The difference in the strength of northward winds is presumably associated with the difference in the representation of topography. The better-resolution model leads to a more sharply northward steering of winds along western North America and the southerly winds are blocked at southern Alaska, leading to

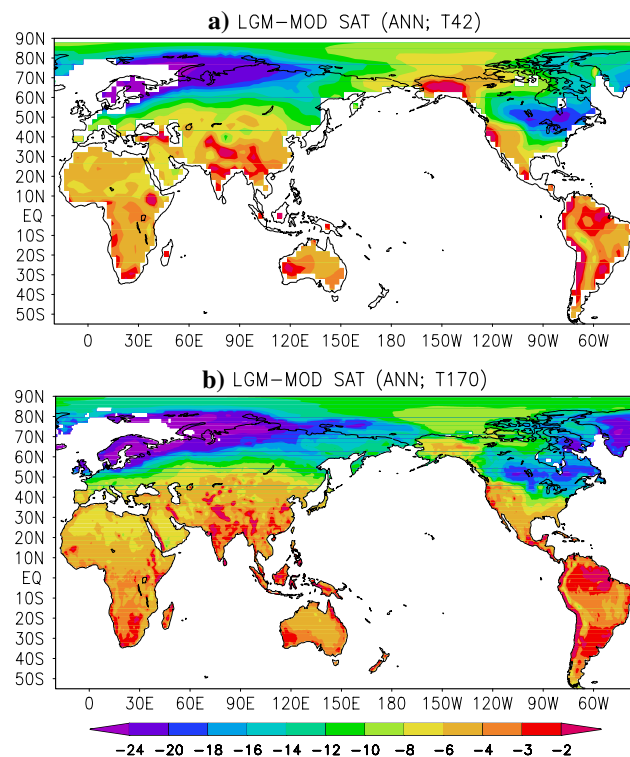


Fig. 3 Geographic distribution of the change in annual-mean surface air temperature simulated in **a** T42 and **b** T170 version

the smaller northward heat transport. On the other hand, in the lower-resolution model southerly winds appear to be more diffuse over Alaska. The smaller northward heat transport in the T170 consequently leads to the colder southward heat transport in northeast of the Hudson Bay and over Greenland. In the south-eastern United States, there is stronger southward heat flux in the T42 than in T170 case, leading to the lower surface temperature than in T170 case. The reason for the difference of southward wind change in the two model versions is not immediately clear. The differences in resolution are also very clear for a number of smaller (but still significant) regions, which simply cannot be adequately resolved at T42 (e.g., Spain, Italy, the British Isles, much of Scandinavia, Indonesia, Japan, New Zealand, Madagascar, and central America).

In order to check the performance of the high-resolution model in comparison to the low-resolution version, we examined the surface air temperature difference in locations where proxy estimates are available (Table 2). When we focus on the proxy estimates that have the greatest reliability (noble gas temperatures from groundwater), results indicate that, although both model temperature estimates are statistically indistinguishable from the observations, $0.5 \pm 0.8^\circ\text{C}$ (T170) and $-0.8 \pm 1.3^\circ\text{C}$ (T42), which represent averages of the surface temperature difference between proxy estimates from ground water noble gas and T170 and T42 simulations listed in Table 2, the T170 has lower error estimates. The same is true for borehole estimates from ice sheets; T170 errors are one-half those of T42. For the best resolved mountain range in the tropics (the Andes), the T170 model in particular has a well-defined cooling of $4\text{--}10^\circ\text{C}$, easily accommodating the ice age reduction in snowline of about 850 m. Results from both of these model runs, but particularly the T170 run, indicate that the longstanding disagreement between LGM tropical SSTs (Webster and Streten 1978; Rind and Peteet 1985) can be explained with a very modest assumption of a $+1^\circ\text{C}$ bias in CLIMAP tropical SSTs and finer model resolution. We also calculated the Student *t* test *p* values to compare how close the proxy data and model results are (Table 3). Over most of the points, the high-resolution temperature differences show a better agreement than those of low-resolution with proxy data. The agreement is especially better over land than in ocean.

Finally, over Antarctica, the largest cooling occurs in the Weddell Sea and the Ross Sea (due to the increase in ice sheet elevation) and the Indian sector of the Southern Ocean partly due to the expansion of sea ice (Fig. 5). The surface cooling is generally larger in western Antarctica than the eastern part due to the larger increase in ice sheet than in the East Antarctica.

Overall, simulated global mean surface air temperature decreases by about 6.1°C in December–January–February,

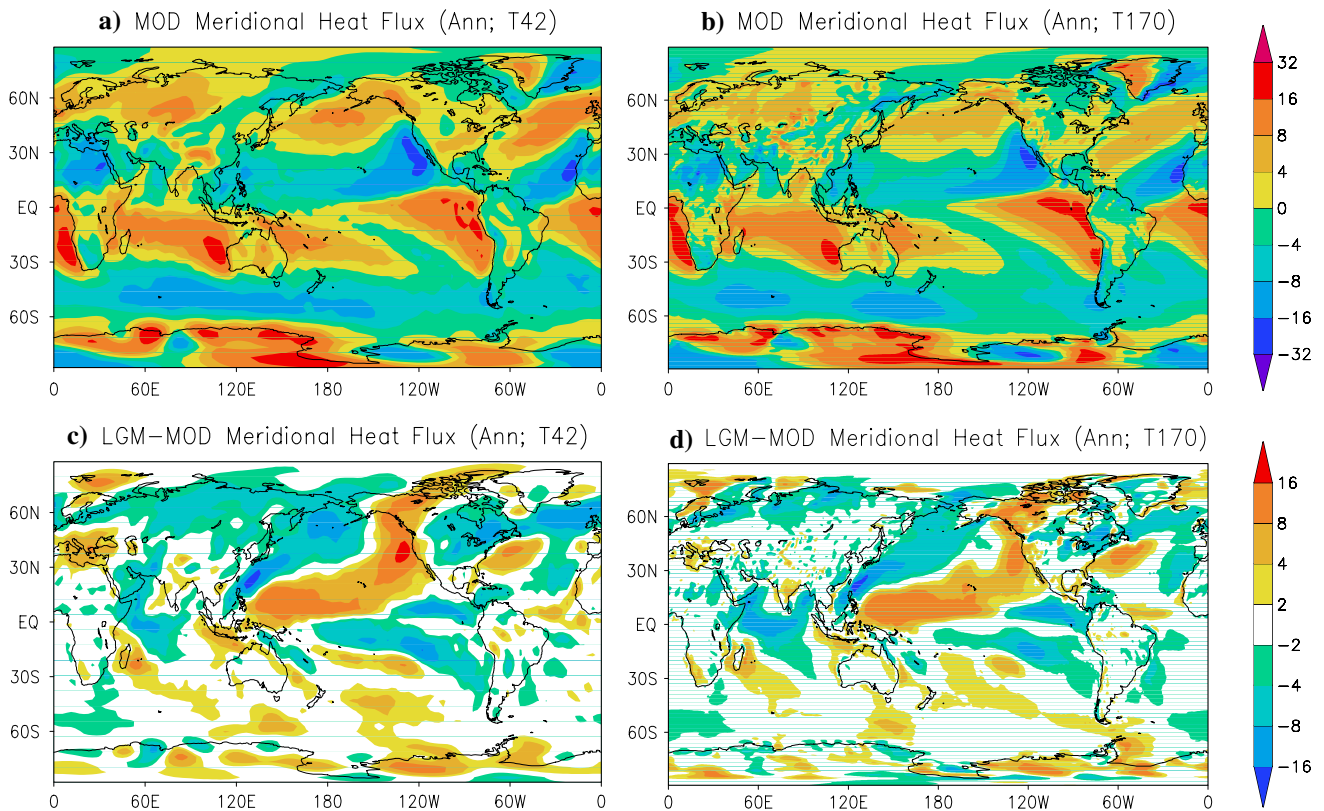


Fig. 4 Geographic distribution of the annual-mean meridional heat flux in **a** MOD simulated in T42, **b** LGM simulated in T170, **c** change between MOD and LGM simulated in T42, and **d** change between MOD and LGM simulated in T170. Units are in km s^{-1}

5.7°C in June–July–August, and 5.9°C (annual) for the high-resolution simulation. These values are virtually identical to the T42 run and not surprisingly indicate that the primary benefit from T170 comes on the regional scale.

3.3 South Asian monsoon

In a further comparison of the high and lower resolution models, we examine the differences in summer precipitation between T42 and T170 version over south Asia, where the summer monsoon is of special interest and where large LGM decreases have been documented (Fig. 6). Terrestrial records from Asia and Africa and marine records from the Indian Ocean indicate a significant weakening of the summer (southwest) monsoon during glacial times (Cullen 1981; Street-Perrott and Perrott 1990; Porter et al. 1992; An et al. 1993; Winkler and Wang 1993; Sirocko et al. 1993; Overpeck et al. 1996; Wang et al. 2001).

Many previous model simulations obtained a weaker southwest monsoon with glacial conditions (Kutzbach and Guetter 1986; Prell and Kutzbach 1987, 1992). However, the GFDL coupled model Bush (2002) and using CCM3 Toracinta et al. (2004) obtained an enhanced southwest monsoon with glacial boundary conditions. The main

difference between our result and that of Toracinta et al. (2004) in the summer monsoon seems to be due to the different treatment of the SST. Toracinta et al. (2004) reduced CLIMAP SST by 4°C in the tropics (see above discussion) and obtained an increase in the sea level pressure over the Arabian Sea and decrease over the Asian continent.

Even though there are general similarities in the precipitation change pattern between our T42 and T170 simulations, some differences exist. The most striking differences involve the clear linkage of T170 anomalies to topography or geography, whereas the T42 anomalies are more like “floating blobs.” For example, the areas of high precipitation in the T170 run can easily be associated with the Eastern Ghats in southeast India, the Ganges Plain in front of the highest part of the Himalayan Front ($>8,000$ m), and the southeast projection of the Himalayan range along $\sim 100^{\circ}\text{E}$. Almost none of these features are clearly resolvable at T42. The positive precipitation anomaly at $\sim 90^{\circ}\text{E}$ in the T42 model runs almost orthogonal to the Himalayan front—a physical response that we find enigmatic at best.

Specific regional anomalies in southeast Asia shown in the T170 panel bear considerable resemblance to paleoclimate reconstructions (Gathorne-Hardy et al. 2002) based

Table 2 Annual-mean surface air temperature difference between LGM and MOD, and proxy estimates and model output of T170 and T42 versions. Differences are negative

No.	Location	ΔT (obs)	ΔT (T170)	$\delta\Delta T$ (T170)	ΔT (T42)	$\delta\Delta T$ (T42)	Proxy method	Source
1	72.6°N, 38.5°W	21	23	-2.0	16	+4.0	Borehole	Cuffey et al. (1995)
2	72.6°N, 37.6°W	21	23	-2.0	17	+3.0	Borehole	Dahl-Jensen et al. (1998)
3	78.3°S, 106.5°E	15	13	+2.0	9.5	+5.5	Borehole	Salamatin et al. (1998)
4	28.5°S, 137°E	9	5.3	+3.7	4.6	+4.4	Emu eggshells	Miller et al. (1997)
5	29.1°N, 98.8°W	5.2	5	+0.2	6.9	-1.7	Noble gas	Stute et al. (1992)
6	36.5°N, 108°W	5.5	6.1	-0.6	4.3	+1.2	Noble gas	Stute et al. (1995a)
7	7°S, 41.5°W	5.4	3.6	+1.8	4.2	+1.2	Noble gas	Stute et al. (1995b)
8	10°N, 106°E	5	4.1	+0.9	5.8	-0.8	Noble gas	Stute et al. (1997)
9	11°N, 13°E	6.4	4.9	+1.5	6.6	-0.2	Noble gas	Edmunds et al. (1998)
10	33°N, 83°W	4.3	5.3	+1.0	6.9	-2.6	Noble gas	Clark et al. (1997)
11	39°N, 76°W	9	9	0.0	9.9	-0.9	Noble gas	Aeschbach-Hertig et al. (1996)
12	23.5°N, 58°E	6.5	5.4	+1.1	7.9	-1.4	Noble gas	Weyhenmeyer et al. (2000)
13	43.5°N, 1.5°W	5.7	5.8	-0.1	6.5	-0.8	Noble gas	Kageyama et al. (2001)
14	48°N, 21°E	8.7	9.2	-0.5	10.7	-2.0	Noble gas	
15	0.27°N, 66.7°W	5-6	2.4	+3.1	3.1	+2.4	Pollen	Colinvaux et al. (1996)
16	4.9°N, 74.33°W	3-4	2.8	+0.7	1.1	+2.4	Pollen	Farrera et al. (1999)
17	16°S, 69°W	5-7	5.8	+0.2	0.8	+5.2	Pollen	
18	3.5°S, 29.57°E	5-6	4.1	+1.4	4.2	+1.3	Pollen	
19	24.43°S, 28.75°E	5-6	2.2	+3.3	4.3	+1.2	Pollen	
20	0.03°N, 37.47°E	5.1-8.8	5.9	+1.1	4.7	+2.3	Pollen	
21	20.08°S, 43.37°W	5-7	4	+2.0	3.2	+2.3	Pollen	
22	22°N, 100.5°W	1.5-3	3.7	-1.45	1.7	+0.55	Pollen	
23	27.68°N, 85.4°E	6-8	4.8	+2.2	5.2	+1.8	Pollen	
24	47°N, 38.5°E	20	7.6	+12.4	7.5	+12.5	Pollen	Kageyama et al. (2001)
25	47°N, 6°E	9	8.1	+0.9	8.6	+0.4	Pollen	
26	55°N, 83°E	10	9.8	+0.2	9.8	+0.2	Pollen	Tarasov et al. (1999)
27	55.17°N, 57.58°E	8	8.1	-0.1	7.9	+0.1	Pollen	
28	47.52°N, 111.27°E	10	5.3	+4.7	7.5	-2.5	Pollen	
29	51.21°N, 99.45°E	5	5.9	-0.9	7.9	-2.9	Pollen	
30	3.2°N, 50.4°E	1.5	1.8	-0.3	1.9	-0.4	Alkenone	Bard et al. (1997)
31	1°N, 139°W	0.5	2.4	-1.9	2.4	-1.9	Alkenone	Lyle et al. (1992)
32	0°, 23°W	1.8	3.9	-2.1	4.3	-2.5	Alkenone	Sikes and Keigwin (1994)
33	25.02°N, 16.65°W	4.5	9.1	-4.6	7.7	-3.2	Alkenone	Ternois et al. (2000)
34	21.48°N, 17.95°W	2-2.5	9.8	-7.55	10.3	-8.05	Alkenone	
35	13.2°N, 59.3°W	5	3	+2.0	3	+2.0	Coral	Guilderson et al. (1994)
36	14.52°S, 117.1°E	0.4	5.4	-5.0	5.8	-5.4	Faunal	Barrows et al. (2000)
37	33.38°S, 161.61°E	4.2	3.4	+0.8	3.4	+0.8	Faunal	
38	44.26°S, 150°E	3.3	3.6	-0.3	3.8	-3.5	Faunal	
39	16.01°S, 76.33°W	6-9	1.5	+6.0	0.8	+6.7	Faunal	Feldberg and Mix (2002)
40	0°, 15°W	5	3.8	+1.2	3.7	+1.3	Faunal	Mix et al. (1999)
41	10°N, 40°W	2-3	2.6	-0.1	2.8	-0.3	Faunal	
42	3°S, 82°W	4-5	2	+2.5	0.1	+4.4	Faunal	
43	1°S, 110°W	2-3	1.2	+1.3	1.3	+1.2	Faunal	
44	42°N, 130.01°W	3.5	4.7	-1.2	4.9	-1.4	Faunal	Ortiz et al. (1997)
45	21.36°N, 158.19°W	2	0	+2.0	0.3	+1.7	Faunal, $\delta^{18}\text{O}$	Lee and Slowey (1999)
46	0.3°N, 159.4°E	2.8	3.3	-0.5	3.2	-0.4	Mg/Ca	Lea et al. (2000)
47	2.3°N, 91°W	2.6	2	+0.6	2.3	+0.3	Mg/Ca	
48	43.22°S, 11.74°E	4-5	3.8	+0.7	5.2	-0.7	Radiolaria	Brathauer and Abelmann (1999)
49	49°S, 12.7°W	3-4	7.8	-4.3	8.8	-5.3	Radiolaria	
50	3.2°N, 101.43°W	3.2	1.2	+2.0	1.3	+1.9	Radiolaria	Pisias and Mix (1997)
51	16.45°S, 77.57°W	3.7	2	+1.7	2.2	+1.5	Radiolaria	

Table 3 Annual-mean surface air temperature difference (LGM-MOD) of proxy estimates and model output for all points (51), land points (29), and ocean points (22)

	All	Land	Ocean
Proxy	6.1	8.2	3.2
T170	5.5 (0.55)	7.0 (0.37)	3.5 (0.62)
T42	5.4 (0.40)	6.7 (0.20)	2.6 (0.58)

Differences are negative. Listed italics in parentheses are student *t* test *p* values comparing the high-resolution and low-resolution model output to those estimated from proxy data

on palynological, geological, fossil, and termite data (a similar pattern is broadly reproduced in the T42, but the relationship to topography is not as well defined). Gathorne-Hardy et al. (2002) suggested that during the LGM most of Thailand, Peninsular Malaysia, western and southern Borneo, eastern and southern Sumatra, and Java were probably covered by savannah, and that rainforest refugia were probably present in northern and eastern Borneo, northern and western Sumatra, and the Mentawai Islands. The sign of the JJA precipitation anomaly in Fig. 6 is consistent with all these changes except for the Malay Peninsula (mixed pattern in the T170 run) and the Mentawai Islands, which the model cannot resolve.

3.4 North American sector

We focus on the North American/North Atlantic sector to examine in more detail regional features in the T170 simulation. One of the most interesting features is the response of the westerly jet over North America associated with the presence of the Laurentide ice sheet (Fig. 7). Some early LGM simulations indicated that the North American ice sheet split the jet stream with one branch flowing around the northern edge and another flowing along the southern edge of the ice sheet (Kutzbach and Wright 1985; Kutzbach and Guetter 1986). From sensitivity experiments applying different elevations of the Laurentide ice sheet, it was believed that the splitting of the jet stream is caused by ice sheet orography and depends on the elevation of the ice sheet (Rind 1987; Shinn and Barron 1989; Bromwich et al. 2004). However, some recent GCM studies of the LGM show little indication of the split upper level jet stream over the Laurentide ice sheet, even if it were as high as CLIMAP (Felzer et al. 1996; Hall et al. 1996; Toracinta et al. 2004).

Figure 7 compares the upper level atmospheric circulation at 300 hPa for the MOD and LGM in DJF simulated in T42 with T170. In winter, the westerly jet becomes stronger over North America and the North Atlantic and extends farther north over western North America in both

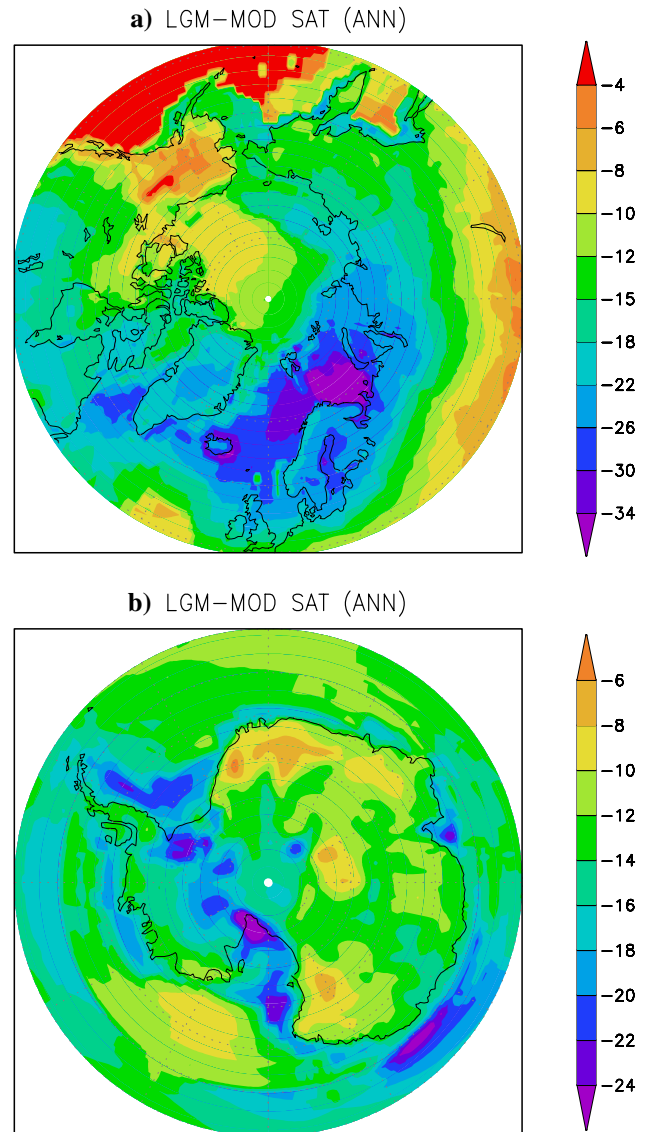


Fig. 5 Geographic distribution of the change in annual-mean surface air temperature for **a** northern polar region and **b** southern polar region

model versions. Over Alaska the south-westerly wind in the MOD is more southerly in the LGM, and this northern branch of the jet blows along the northern rim of the Laurentide ice sheet. There is also a southern branch of the jet over Mexico, which meets the northern branch in the North Atlantic along the main storm track.

Compared to the previous simulation by Kutzbach and Wright (1985), the northern and southern branches are located somewhat farther to the south in this study and the southern branch is weaker. Whereas Kutzbach and Wright (1985) obtained the westerly splitting in summer, the splitting is not found in this study (not shown). Using NCAR mesoscale model (Polar MM5), Bromwich et al. (2004) also simulated the splitting of the westerly jet only

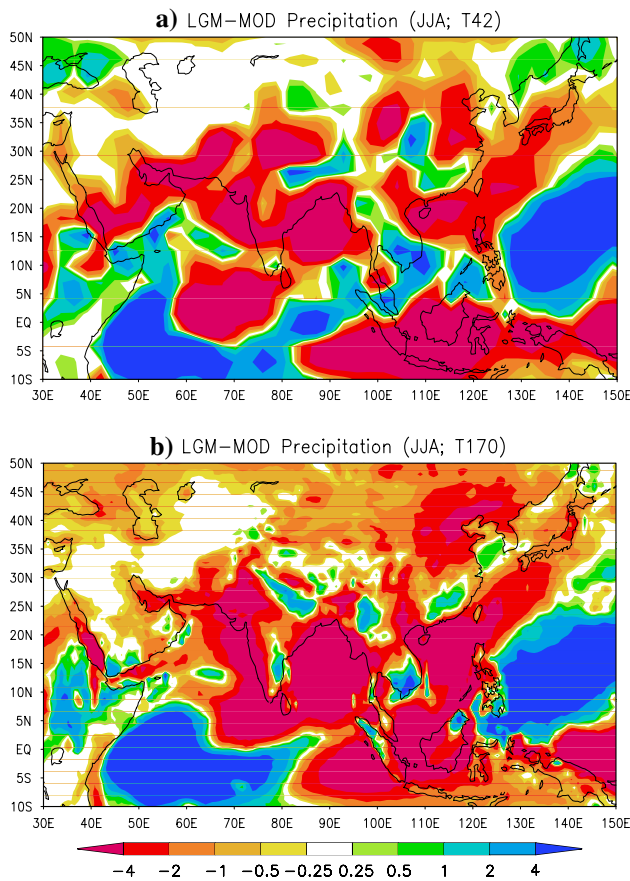


Fig. 6 Geographic distribution of the change in summer precipitation over Asia simulated in **a** T42 and **b** T170 version. Units are in mm day^{-1}

in winter as in this study, but the splitting is much more pronounced and the northern branch is stronger than this study. The difference between these previous studies and this study seems to be associated with the difference in the representation of the ice sheet orography over North America. The result obtained in this study indicates that a modified splitting of the westerly jet over North America persists even with the lower elevation Laurentide ice sheet than that suggested by CLIMAP. Because the level of splitting appears to be dependent in part on elevation of the Laurentide Ice Sheet, we postulate that the Ice-5G reconstruction (Peltier 2004), with a significant ice dome west of Hudson's Bay, might produce even greater amplifications of the jet (and greater wave number one extremes—see below) than the one we simulate.

The increase in southerly flow over western North America leads to a poleward atmospheric heat transport greater than the present in this region (Fig. 4c, d). The perturbation of the flow is sufficiently large to cause a wave number-one polarity in the polar heat anomalies, with the Eurasian sector being much colder than the North American sector (Figs. 3, 5a). The temperatures over Greenland

are consistent with borehole measurements by Cuffey and Clow (1997; see also Table 2).

The changes in circulation lead to changes in model precipitation (Fig. 8). In both seasons, precipitation decreases over Canada and large parts of the North Atlantic, plus the Gulf of Mexico and Florida (the latter two especially in summer). Precipitation increases over the western US and western Mexico, and in the eastern US along the trend of the Appalachian Mountains and eastward of the mountains. This feature is more distinct in the T170 case. The increase in winter precipitation over the western US is associated with the deepening of the Aleutian low pressure in winter and the weakening of North Pacific high pressure system in summer (not shown). Bromwich et al. (2004, 2005) also obtained a large precipitation along the western margin of North America in their LGM simulation, which they attributed to the frequent development of cyclones over coastal Beringia and Alaska, and in the Gulf of Mexico and the eastern margin of North America along the southern branch of the jet stream. This is verified in our run by a more detailed analysis of the winter circulation (Unterman 2007).

The better resolution of geography in the T170 model enables more precise placement of the locations of western DJF precipitation maxima as being in the Great Valley of California, a line running from SE to NW Arizona and centered roughly on the central reaches of the Colorado River, and an extension eastward to $\sim 100^\circ\text{W}$ into the southern High Plains (including the Edwards Plateau of Texas) (Fig. 8a, d). DJF precipitation decreases in eastern North America in a region parallel to and west of the Appalachians; this is associated with the southward expansion of the upper level trough (not shown) that parallels the northward expansion farther to the west.

The JJA moisture pattern over much of North America east of the Rocky Mountains and south of the ice sheet is due to a stronger subtropical high-pressure system over the North Atlantic, that is stretched along a southwest-northeast axis (not shown), with orographic precipitation on the eastern (windward) slope of the Sierra Madre Occidentale. There is also a region of stronger center of precipitation restricted to a $10\text{--}20^\circ$ corridor in the Maritime Provinces of Canada, between the ice sheet/sea ice boundary on the northwest and a very strong subtropical high to the southeast (not shown). Bromwich et al. (2004, 2005) obtained a maximum summertime precipitation in the southern margin of the Laurentide ice sheet in response to the northward displacement of the jet stream and associated cyclone frequencies.

The mean annual P-E pattern shows the net effect of the precipitation and temperature changes on moisture availability (Fig. 8c, f). The pattern generally reflects the above discussed precipitation changes, except that in the western US during the LGM, the region of net moisture gain is

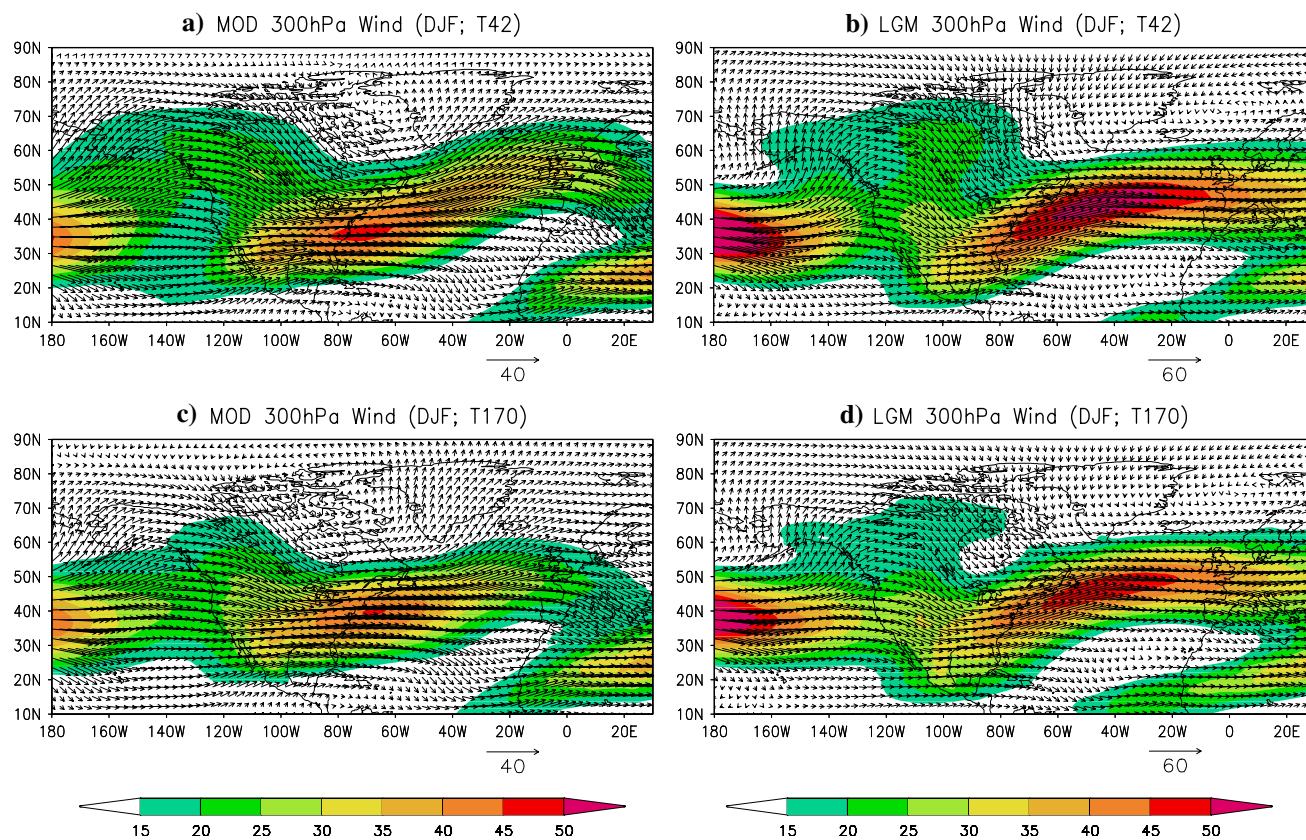


Fig. 7 Geographic distribution of the winter wind vectors at 300 hPa for **a** MOD and **b** LGM in T42, and **c** MOD and **d** LGM in T170 version. Units are in m s^{-1}

restricted to the Western Cordillera region. The sub-parallel zones of maximum net moisture gain are in the Sacramento Basin (cf. above discussion), the SE-NW line from about 32°N and 109°W to 43°N , 116°W and encompassing virtually the entire Colorado River Basin and the upper reaches of the Snake River Plain in Idaho. A third smaller region of meteorological interest involves a small tongue originating at about 37°N , 108°W and curling north-northwest around the highest part of Front Range of the Rockies from the Medicine Bow Mountains in southern Wyoming to the Sangre de Cristo Mountains in north-central New Mexico. Although the large-scale significance of this response may be minor, it may be worth examining more because of its meteorological interest.

Except for Florida, which is dominated by unusual summertime aridity, most of the rest of the eastern US is wetter than present in the annual mean. A comparison with a change in hydrological budget indicates that the net moisture increase west of the Appalachians is due to the larger reduction in evaporation (not shown) over precipitation associated with the surface cooling by up to about 10°C in comparison to present (Fig. 3). East of the mountains the precipitation increase certainly plays a role in the net moisture surplus. The increase in P-E over

southern Canada including the Great Lakes is due to a larger reduction in evaporation (not shown) than that in precipitation due to the marked surface cooling over the Laurentide Ice Sheet (see Fig. 3).

The above results indicate that the regional climate changes simulated by the T170 is different from the lower resolution models because those models cannot resolve the types of topographic features that are highlighted above—not only with respect to the major uplifted terrains of the Sierra Nevada and Colorado Rockies but also with respect to the Appalachian Mountains. Without going into exhaustive detail, we note that these results are in many cases consistent with proxy evidence. Enhanced Florida aridity is consistent with evidence from central Florida of a low water table during the LGM (Watts 1983). Lake level data and pollen and plant microfossils have long indicated that the now-arid regions of the western US were generally wetter in the LGM (e.g., Farrera et al. 1999; Kohfeld and Harrison 2000). Our estimates of $0.5\text{--}1.0\text{ mm/year}$ net moisture surplus are valuable for more quantitative testing against hydrological models of some of the large lakes in the Great Basin of Utah, such as Lake Lahontan/Great Salt Lake. One of us (D. Erickson, in preparation) will be reporting on moisture budget changes in this region, and

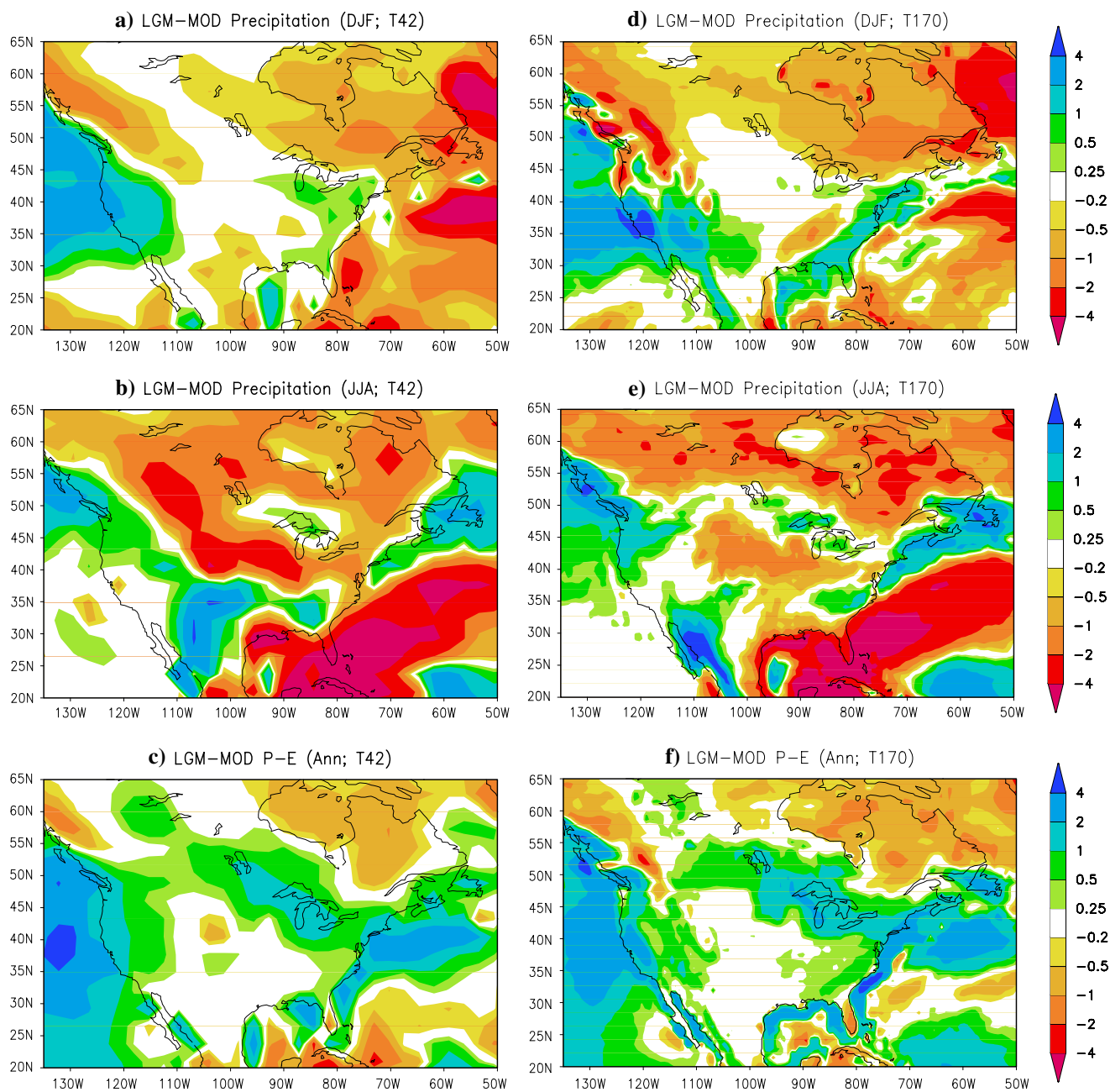


Fig. 8 Geographic distribution of the change in **a** winter and **b** summer precipitation, and **c** annual-mean precipitation minus evaporation simulated in T42 version and **d** winter and **e** summer

precipitation, and **f** annual-mean precipitation minus evaporation simulated in T170 version. Units are in mm day^{-1}

comparison with observations, in more detail at a later time.

Another region of interest for changes in P-E is the North Atlantic where precipitation markedly reduced in the LGM. The inferred salinity increase in the North Atlantic between 30° and 35°N is in the same belt where, during the LGM the Gulf Stream/North Atlantic Current System transported warm water from the tropics to mid- and high-latitudes (Crowley 1981). Explicitly incorporating the

effects of such salinity changes in models may reveal additional insights into the dynamical ocean response of this current system during the LGM.

3.5 African and South American moisture changes

Figure 9 displays the change in P-E in South America and Africa in both model versions. In South America, parts of

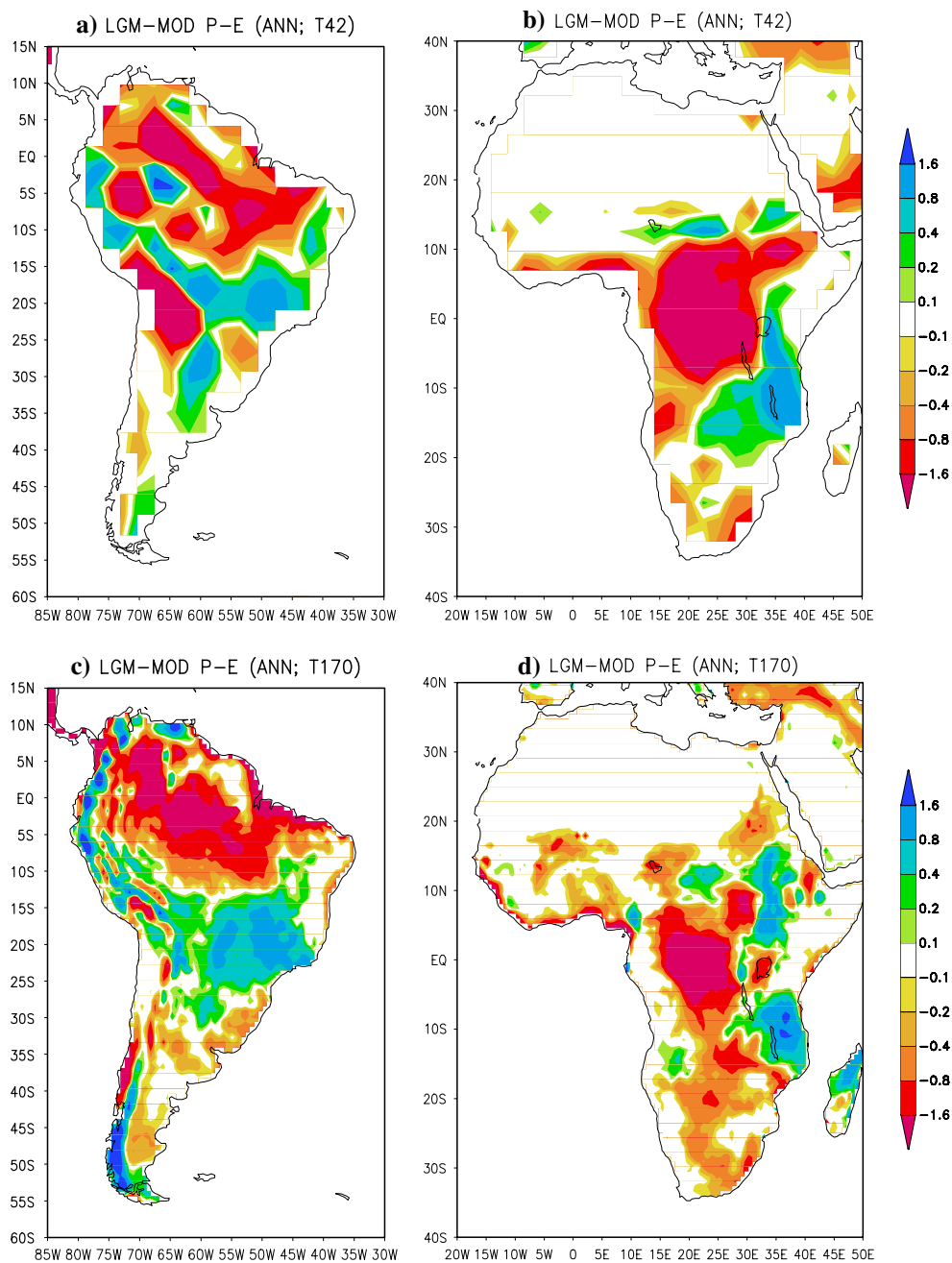


Fig. 9 Geographic distribution of the change in annual-mean precipitation minus evaporation for **a** South America and **b** Africa simulated in T42 version and **c** South America and **d** Africa simulated in T170 version. Units are in mm day^{-1}

the Amazon are much drier than present, while between 15 and 25°S it is much wetter than present. The drier climate in the Amazon is supported by the change in plant available moisture inferred from pollen, which was less abundant in the LGM than today (Farrera et al. 1999). The precipitation changes are reflected in the changes in cloudiness (not shown), which indicate fewer clouds in the north and more clouds in the band of increased precipitation. The specific circulation features responsible for these changes are not immediately obvious and will be examined in detail in a

later publication. Wetter climate over parts of the high elevation Andean Altiplano was however inferred by Farrera et al. (1999), using pollen and plant microfossil data. A particularly intriguing result is the discrimination of clear climate trends along the narrow coastal strip west of the Andes—a region that is not adequately resolved in the lower resolution simulation as shown in Fig. 10.

In Africa, the central part is drier, consistent with the vegetation reconstruction of Crowley (1995). The increased wetness in the eastern part is consistent with the

proxy evidence by Kohfeld and Harrison (2000) from P-E inferences. In the simulation, there is almost no change in P-E budget over northern Africa, but some paleoclimate proxy evidence suggested this region to be wetter in the LGM (e.g., Farrera et al. 1999). The reason for this difference is not immediately clear.

4 Summary and conclusion

This study explores the response of a high-resolution climate model to the imposition of LGM boundary conditions. The simulations were performed with the NCAR CCM3 atmospheric general circulation model at a spectral truncation of T170, corresponding to a horizontal resolution of about 75 km. We performed a parallel T42 run to examine whether there are benefits from increasing the resolution. In the modern climate simulation, the precipitation appears to be realistic in its pattern and magnitude compared to observations. In particular, the high-resolution model reproduces the heavy precipitation belt in the tropical Pacific associated with ITCZ reasonably well, which is an important climate factor difficult to resolve in most climate models.

From a comparison of the surface air temperature from proxy data to that simulated in the T170 and T42 model versions, the high-resolution temperature differences show a better agreement than those of the low-resolution model, especially over land. Comparison of model temperature

estimates with the best-constrained proxy temperature estimates (noble gases from groundwater) indicates no significant differences, thereby apparently resolving a longstanding model-data difference. Summer precipitation change over Asia simulated in high-resolution model shows a clear differences with the low-resolution version associated with a linkage to topography in areas such as southeast India and the Himalayas.

In the LGM simulation, one of the most interesting features is the splitting of the upper level westerly jet around the Laurentide ice sheet into northern and southern branches over North America, especially in northern winter. In the hydrological budget change pattern, the T170 simulation enables a finer level of discrimination of topographic features than in earlier runs, thus opening the door for more precise validation of model results. In particular, it is clear that even subdued features such as the Appalachian Mountains may result in significant differences in regional climate response that just could not be discriminated at a lower level of resolution.

Much more could be commented on regarding these simulations. An obvious area for future simulations would involve the role of land vegetation/land use change (cf. Crowley and Baum 1997) and uncertainties in our results due to uncertainties in boundary conditions (particularly sea ice and SST). But this paper sets out the major justification and highlights of some of the many benefits that can be obtained from higher resolution simulations of the ice age world. The results also provide a “model data” base that is on approximately the same scale as many geological data and one that we plan to release at the time of publication of this paper.

Acknowledgments We wish to thank Oak Ridge National Laboratory of the U.S. for model computation. The authors would also like to acknowledge the support from Korea Institute of Science and Technology Information (KISTI) under ‘The Eighth Strategic Supercomputing Support Program’ with Dr. Sang-Min Lee as the technical supporter. Jesse Kenyon at Duke University is especially appreciated for his valuable comments in improving the manuscript. Constructive comments from anonymous reviewers are also appreciated. Oak Ridge National Laboratory is managed by UT-Battelle, LLC, for the U.S. Department of Energy under Contract DE-AC05-00OR22725. This study was supported by projects of Integrated Research on the Composition of Polar Atmosphere and Climate Change (COMPAC) (PE07030) and Polar Science program of Korea Science and Engineering Foundation (R01-2006-000-10441-0). Some of this work was supported by an NSF grant to Thomas J. Crowley at Duke University.

References

- Aeschbach-Hertig W, Stute M, Schlosser P, Clark J, Reuter R (1996) Large (9°) glacial–interglacial temperature difference derived from an aquifer in Maryland (abstract). *Eos Trans AGU Spring Meet Suppl* 77(17):157

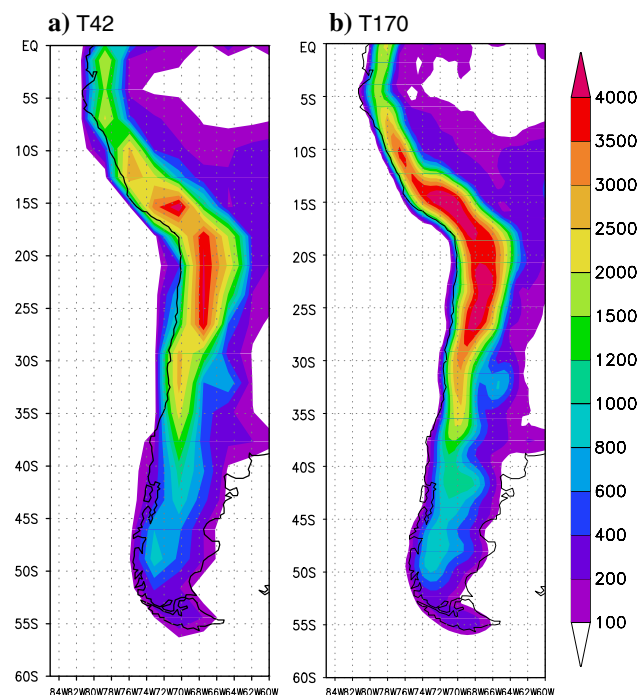


Fig. 10 Geographic distribution of the topography over Southwest America used in **a** T42 and **b** T170 version of the model

- An Z, Stephen CP, Zhou W, Lu Y, Douglas JD, MJ Head, Wu X, Ren J, Zheng H (1993) Episode of strengthened summer monsoon climate of younger Dryas Age on the Loess Plateau of Central China. *Quat Res* 39:45–54
- Ballantyne AP, Lavine M, Crowley TJ, Liu J, Baker PB (2005) Meta-analysis of tropical surface temperatures during the Last Glacial Maximum. *Geophys Res Lett* 32:L05712
- Bard E, Rostek F, Sonzogni (1997) Interhemispheric synchrony of the last deglaciation inferred from alkenone palaeothermometry. *Nature* 385:707–710
- Barrows TT, Juggins S, De Deckker P, Thiede J, Martinez JI (2000) Sea-surface temperatures of the southwest Pacific Ocean during the last glacial maximum. *Paleoceanography* 15:95–109
- Berger A (1978) Long-term variations of daily insolation and quaternary climate changes. *J Atmos Sci* 35:2362–2367
- Bonan G (1998) The land surface climatology of the NCAR Land Surface Model coupled to the NCAR Community Climate Model. *J Clim* 11:1307–1326
- Braithauer U, Abelmann A (1999) Late quaternary variations in sea surface temperatures and their relationship to orbital forcing recorded in the Southern Ocean (Atlantic sector). *Paleoceanography* 14:135–148
- Broccoli AJ (2000) Tropical cooling at the last glacial maximum: an atmosphere-mixed layer ocean model simulation. *J Clim* 13:951–976
- Bromwich DH, Toracinta ER, Wei H, Oglesby RJ, Fastook JL, Hughes TJ (2004) Polar MM5 simulations of the winter climate of the Laurentide ice sheet at the LGM. *J Clim* 17:3415–3433
- Bromwich DH, Toracinta ER, Oglesby RJ, Fastook JL, Hughes TJ (2005) LGM summer climate on the southern margin of the Laurentide ice sheet: wet or dry? *J Clim* 18:3317–3338
- Burckle LH, Robinson D, Cooke D (1982) Reappraisal of sea ice distribution in Arlantic and Pacific sectors of the Southern Ocean at 18,000 yr BP. *Nature* 299:435–437
- Bush ABG (2002) A comparison of simulated monsoon circulations and snow accumulation in Asia during the mid-Holocene and at the last glacial maximum. *Global Planet Change* 32: 331–347
- Clark JF, Stute M, Schlosser P, Drenkard S, Bonani G (1997) A tracer study of the Floridan aquifer in southeastern Georgia: Implications for groundwater flow and paleoclimate. *Water Resour Res* 33:281–289
- Clark PU, Mix AC, Bard E (2001) Ice sheets and sea level of the last glacial maximum. *EOS Trans AGU* 82(22):241–247
- CLIMAP (1976) The surface of the ice-age earth. *Science* 191: 1131–1136
- CLIMAP (1981) Seasonal reconstructions of the Earth's surface at the last glacial maximum. *Geol Soc Amer Map Chart Ser, MC-36*
- Colinvaux PA, Deoliveria PE, Moreno JE, Miller MC, Bush MB (1996) A long pollen record from lowland Amazonia: forest and cooling in glacial times. *Science* 274:85–88
- Crowley TJ (1981) Temperature and circulation changes in the eastern North Atlantic during the last 150,000 years: evidence from the planktonic foraminiferal record. *Mar Micropaleontol* 6:97–129
- Crowley TJ (1995) Ice age terrestrial carbon changes revisited. *Global Biogeochem Cycles* 9:377–389
- Crowley TJ (2000) CLIMAP SSTs revisited. *Clim Dyn* 16:241–255
- Crowley TJ, Baum SK (1997) Effect of vegetation on an ice-age climate model simulation. *J Geophys Res* 102:16463–16480
- Crowley TJ, Parkinson CL (1988) Late Pleistocene variations in Antarctic sea ice, I, Effect of orbital insolation changes. *Clim Dyn* 3:85–91
- Cuffey KM, Clow GD (1997) Temperature, accumulation, and ice sheet elevation in central Greenland through the last deglacial transition. *J Geophys Res* 102:26383–26396
- Cuffey KM, Clow GD, Alley RB, Stuiver M, Waddington ED, Saltus RW (1995) Large Arctic temperature change at the Wisconsin-Holocene glacial transition. *Science* 270:455–458
- Cullen JL (1981) Microfossil evidence fro changing salinity patterns in the Bay of Bengal over the last 20,000 years. *Palaeogeogr Paleoclimatol Palaeoecol* 35:315–356
- Dahl-Jensen D, Mosegaard K, Gundestrup N, Clow GD, Johnsen SJ, Hansen AW, Balling N (1998) Past temperatures directly from the Greenland ice sheet. *Science* 282:268–271
- Duffy PB, Govindasamy B, Iorio JP, Milovich J, Sperber KR, Taylor KE, Wehner MF, Thompson SL (2003) High-resolution simulations of global climate, part 1: present climate. *Clim Dyn* 21:371–390
- Edminds WM, Fellman E, Goni IB, McNeill G, Harkness DD (1998) Groundwater paleoclimate and paleorecharge in the SW Chad Baxin, Borneo State, Nigeria. In: *Isotope techniques in studying past and current environmental changes in the hyfrosphere and atmosphere*. IAEA, Vienna
- Fairbanks RG (1989) A 17000-year glacio-eustatic sea level record: influence of glacial melting rates on the Younger Dryas event and deep-ocean circulation. *Nature* 342:637–642
- Farrera I, Harrison SP, Prentice IC, Ramstein G, Guiot J, Bartlein PJ, Bonnefille R, Bush M, Cramer W, von Grafenstein U, Holmgren K, Hooghiemstra H, Hope G, Jolly D, Lauritzen S-E, Ono Y, Pinot S, Stute M, Yu G (1999) Tropical climates at the last glacial maximum: a new synthesis of terrestrial paleoclimate data, I Vegetation, lake-levels and geochemistry. *Clim Dyn* 15:823–856
- Feldberg MJ, Mix AC (2002) Sea-surface temperature estimates in the Southeast Pacific based on planktonic foraminiferal species: Modern calibration and Last Glacial Maximum. *Mar Micropaleontol* 44:1–29
- Felzer B, Oglesby RJ, Webb T III, Hyman DE (1996) Sensitivity of a general circulation model to changes in northern hemisphere ice sheets. *J Geophys Res* 101:19077–19092
- Ganopolski A, Rahmstorf S, Petoukhov V, Claussen M (1998) Simulation of modern and glacial climates with a coupled global model of intermediate complexity. *Nature* 391:351–356
- Gates WL (1976) Modelling the ice-age climate. *Science* 191: 1138–1144
- Gathorne-Hardy FJ, Syaukani, Davies RG, Peggleton P, Jones DT (2002) Quaternary rainforest refugia in south-east Asia: using termites (Isoptera) as indicators. *Biol J Linnean Soc* 75:453–466
- Guilderson TP, Fairbanks RG, Rubenstone JL (1994) Tropical temperature variations since 20,000 years ago: modulating interhemispheric climate change. *Science* 263:663–665
- Hack JJ, Kiehl JT, Hurrell JW (1998) The hydrologic and thermodynamic characteristics of the NCAR CCM3. *J Clim* 11:1179–1206
- Hall N MJ, Valdes PJ, Dong B (1996) The maintenance of the last great ice sheets: A UGAMP GCM Study. *J Clim* 9:1004–1019
- Hewitt CD, Broccoli AC, Mitchell JF, Stouffer RJ (2001) A coupled model study of the last glacial maximum: was part of the North Atlantic relatively warm? *Geophys Res Lett* 28:1571–1574
- Hines KM, Bromwich DH, Rasch PJ, Iacono MJ (2004) Antarctic clouds and radiation within the NCAR climate model. *J Clim* 17:1198–1212
- Hyde W, Crowley TJ, Kim K-Y, North G (1989) Comparison of GCM and energy balance model simulations of seasonal temperature changes over the past 18 000 years. *J Clim* 2: 864–887
- Joussaume S, Taylor KE (2000) The paleoclimate modeling inter-comparison project (PIMIP). In: Braconnot P (ed) *Proceedings of the third PIMIP Workshop*, Canada, pp 9–24
- Kageyama M, Peyron O, Pinot S, Tarasov P, Guiot J, Joussaume S, Ramstein G (2001) The last glacial maximum climate over

- Europe and western Siberia: a PMIP comparison between models and data. *Clim Dyn* 17:23–43
- Kageyama M, Laine A, Abe-Ouchi A, Braconnot P, Cortijo E, Crucifix M, de Vernal A, Guiot J, Hewitt CD, Kitoh A, Kucera M, Marti O, Oghaito R, Otto-Bliesner B, Peltier WR, Rosell-Mele A, Vettoretti G, Weber SL, Yu Y, MARGO Project Members (2006) Last Glacial Maximum temperatures over the North Atlantic, Europe and western Siberia: a comparison between PMIP models, MARGO sea-surface temperatures and pollen-based reconstructions. *Quat Sci Rev* 25:2082–2102
- Kiehl JT, Hack JJ, Bonan BG, Boville BA, Williamson DL, Rasch P (1998a) The National Center for atmospheric research community climate model: CCM3. *J Clim* 11:1131–1149
- Kiehl JT, Hack JJ, Hurrell J (1998b) The energy budget of the NCAR community climate model: CCM3. *J Clim* 11:1151–1178
- Kim S-J, Flato GM, Boer GJ, McFarlane NA (2002) A coupled climate model simulation of the last glacial maximum, Part 1: Transient multi-decadal response. *Clim Dyn* 19:515–537
- Kim S-J, Flato GM, Boer GJ (2003) A coupled climate model simulation of the last glacial maximum, Part 2: approach to equilibrium. *Clim Dyn* 20:635–661
- Kitoh A, Murakami S, Koide H (2001) A simulation of the last glacial maximum with a coupled atmosphere–ocean GCM. *Geophys Res Lett* 28:2221–2224
- Kohfeld KE, Harrison SP (2000) How well can we simulate past climates? Evaluating the models using global paleoenvironmental datasets. *Quat Sci Rev* 19:321–346
- Kutzbach JE, Guetter P (1986) The influence of changing orbital parameters and surface boundary conditions on climate simulations for the past 18000 years. *J Atmos Sci* 43:1726–1738
- Kutzbach JE, Wright HE Jr (1985) Simulation of the climate of 18,000 yr BP: results for the North American/North Atlantic/European sector and comparison with the geologic record. *Quat Sci Rev* 4:147–187
- Lea DW (2004) The 100,000-yr cycle in tropical SST, greenhouse forcing, and climate sensitivity. *J Clim* 17:2170–2179
- Lee KE, Slowey NC (1999) Cool surface waters of the subtropical North Pacific Ocean during the last glacial. *Nature* 397:512–514
- Lea DW, Pak DK, Spero HJ (2000) Quaternary equatorial Pacific sea surface temperature variations. *Science* 289:1719–1724
- Lyle MW, Prahl FG, Sparrow MA (1992) Upwelling and productivity changes inferred from a temperature record in the central equatorial Pacific. *Nature* 355:812–815
- Manabe S, Hahn DG (1977) Simulation of the tropical climate of an ice age. *J Geophys Res* 82:3889–3911
- McIntyre A et al (1976) The glacial North Atlantic 18,000 years ago: a CLIMAP reconstruction. In: Clime RM, Hays JD (eds) Investigation of late quaternary paleoceanography and paleoclimatology: Geological Society of America Memoir, vol 145, pp 43–76
- Miller GH, Magee JW, Jull AJT (1997) Low-latitude glacial cooling in the Southern Hemisphere from amino-acid racemization in emu eggshells. *Nature* 385:241–244
- Mix AC, Morey AE, Pisias NG, Hostetler SW (1999) Foraminiferal faunal estimates of paleotemperature: circumventing the no-analog problem yields cool ice age tropics. *Paleoceanography* 14:350–359
- Ortiz J, Mix A, Hostetler S, Kashgarian M (1997) The California current of the last glacial maximum: reconstruction at 42°N based on multiple proxies. *Paleoceanography* 12:191–205
- Otto-Bliesner BL, Esther CB, Caluzet G, Tomas R, Levis S, Kothavala Z (2006) Last glacial maximum and holocene climate in CCM3. *J Clim* 19:2526–2544
- Overpeck J, Anderson D, Trumbore S, Prell W (1996) The southwest Indian monsoon over the last 18,000 years. *Clim Dyn* 12: 213–225
- Peltier WR (1994) Ice age paleotopography. *Science* 265:195–201
- Peltier WR (2004) Global glacial isostasy and the surface of the ice-age earth: the ice-5G (VM2) model and GRACE. *Annu Rev Earth Planet Sci* 32:111–149
- Peltier WR, Solheim LP (2004) The climate of the last glacial maximum: statistical equilibrium state and a mode of internal variability. *Quat Sci Rev* 23:335–357
- Petit JR, Jouzel J, Raynaud D, Barkov NI, Barnola J-M, Basile I, Benders M, Chappellaz J, Davis M, Delayque G, Delmotte M, Kotlyakov VM, Legrand M, Lipenkov VY, Lorius C, Pépin L, Ritz C, Saltzman E, Stievenard M (1999) Climate and atmospheric history of the past 420,000 years from the Vostok ice core, Antarctica. *Nature* 399:429–436
- Pisias NG, Mix AC (1997) Spatial and temporal oceanographic variability of the eastern equatorial Pacific during the late Pleistocene: Evidence from Radiolarian microfossils. *Paleoceanography* 12:381–393
- Porter SC, An Z, Zheng H (1992) Cyclic quaternary alluviation and terracing in a nonglaciated drainage basin on the north flank of the Qinling Shan, central China. *Quat Res* 38:157–169
- Prell WL, Kutzbach JE (1987) Monsoon variability over the past 150,000 years. *J Geophys Res* 92:8411–8425
- Prell WL, Kutzbach JE (1992) Sensitivity of the Indian monsoon to forcing parameters and implications for its evolution. *Nature* 360:647–652
- Rind D (1987) Components of the ice age circulation. *J Geophys Res* 92:4241–4281
- Rind D, Peteet D (1985) Terrestrial conditions and the last glacial maximum and CLIMAP sea surface temperature estimates: are they consistent? *Quat Res* 24:1–22
- Salamatin AN, Lipenkov VY, Barkov NI, Jouzel J, Petit JR, Raynaud D (1998) Ice core age dating and paleothermometer calibration based on isotope and temperature profiles from deep boreholes at Vostok Station (East Antarctica). *J Geophys Res* 103:8963–8977
- Shin S-I, Liu Z, Otto-Bliesner B, Brady E, Kutzbach J, Harrison S (2003) A simulation of the last glacial maximum climate using the NCAR-CCSM. *Clim Dyn* 20:127–151
- Shinn RA, Barron EJ (1989) Climate sensitivity to continental ice sheet size and configuration. *J Clim* 2:1517–1537
- Sigenthaler U, Monnin E, Kawamura K, Spahni R, Schwander J, Stauffer B, Stocker TF, Barnola J-M, Fischer H (2005) Supporting evidence from the EPICA Dronning Maud Land ice core for atmospheric CO₂ changes during the past millennium. *Tellus* 57B:51–57
- Sikes EL, Keigwin LD (1994) Equatorial Atlantic sea surface temperature for the last 30 kyr: a comparison of U₃₇^k, δ¹⁸O and foraminiferal assemblage temperature estimates. *Paleoceanography* 9:31–45
- Sirocko F, Sarnthein M, Erlenkeuser H, Lange H, Arnold M, Duplessy JC (1993) Century-scale events in monsoonal climate over the past 24,000 years. *Nature* 364:322–324
- Street-Perrott FA, Perrott RA (1990) Abrupt climate fluctuations in the tropics: the influence of Atlantic Ocean circulation. *Nature* 343:607–612
- Stute M, Schlosser P, Clark JF, Broecker WS (1992) Paleotemperatures in the southwestern United States derived from noble gases in ground water. *Science* 256:1000–1003
- Stute M, Clark JF, Schlosser P, Broecker WS, Bonani G (1995a) A 30,000 yr continental paleotemperature record derived from noble gases dissolved in groundwater from the San Juan Basin, New Mexico. *Quat Res* 43:209–220
- Stute M, Forster M, Frischkorn H, Serejo A, Clark JF, Schlosser P, Broecker WS, Bonani G (1995b) Cooling of tropical Brazil (5°) during the Last Glacial Maximum. *Science* 269:379–383
- Stute M, Khoi L-V, Schlosser P, Tobin M, Higgins S (1997) Glacial paleotemperature records for the tropics derived from noble

- gases dissolved in groundwater. *Eos Trans Am Geophys Union* 78:F44
- Tarasov P, Coauthors (1999) Last glacial maximum climate of the former Soviet Union and Mongolia reconstructed from pollen and plant microfossil data. *Clim Dyn* 15:227–240
- Ternois Y, Sicre M-A, Paterne M (2000) Climatic changes along the northwestern African continental margin over the last 30 kyrs. *Geophys Res Lett* 27:133–136
- Toracinta ER, Oglesby RJ, Bromwich DH (2004) Atmospheric response to modified CLIMAP ocean boundary conditions during the Last Glacial Maximum. *J Clim* 17:504–522
- Unterman M (2007) High resolution simulation of synoptic scale meteorology for the last glacial maximum. Duke Univ, pp76
- Wang YJ, Cheng H, Edwards RL, An ZS, Wu JY, Shen C-C, Dorale JA (2001) A high-resolution absolute-dated Late Pleistocene monsoon record from Hulu Cave, China. *Science* 294:2345–2348
- Warren SG, Hahn CJ, London J, Chervin RM, Jenne RL (1986) Global distribution of total cloud cover and cloud type amounts over land. NCAR Tech. Note, NCAR/TN-273+STR, 29 pp. + 200 maps
- Warren SG, Hahn CJ, London J, Chervin RM, Jenne RL (1988) Global distribution of total cloud cover and cloud type amounts over the ocean. NCAR Tech. Note, NCAR/TN-317+STR, 41 pp. + 170 maps
- Watts WA (1983) Vegetation history of the eastern United States 250,000 to 10,000 years ago. In: Wright HE Jr (ed) Late-quaternary environment of the United States. University of Minneapolis Press, Minneapolis, pp 294–310
- Weaver AJ, Eby M, Fanning AF, Wiebe EC (1998) Simulated influence of carbon dioxide, orbital forcing and ice sheets on the climate of the last glacial maximum. *Nature* 394:847–853
- Webster PJ, Stretten NA (1978) Late quaternary ice age climates of tropical Australasia: interpretation and reconstructions. *Quat Res* 10:279–309
- Weyhenmeyer CE, Burns SJ, Waber HN, Aeschbach-Hertig W, Kipfer R, Loosli HH, Matter A (2000) Cool glacial temperatures and changes in moisture source recorded in Oman groundwaters. *Science* 287:842–845
- Winkler MG, Wang PK (1993) Late-quaternary vegetation and climate of China. In: Wright HE Jr et al (ed) Global climates since the last glacial maximum. University of Minnesota Press, USA
- Xie P, Arkin PA (1998) Global monthly precipitation estimates from satellite-observed outgoing longwave radiation. *J Clim* 11:137–164
- Yokoyama Y, Lambeck K, De Deckker P, Johnston P, Fifield LK (2000) Timing of the last glacial maximum from observed sea-level minima. *Nature* 406:713–716